Co@CoSb Core–Shell Nanorods: From Chemical Coating at the Nanoscale to Macroscopic Consolidation

Udishnu Sanyal, Semih Ener, Evangelia Anagnostopoulou, Marc Pousthomis, Pier-Francesco Fazzini, Lise-Marie Lacroix, Konstantin Skokov, Oliver Gutfleisch, G. Viau

Co@CoSb core-shell nanorods: from chemical coating at the nanoscale to macroscopic consolidation

Udishnu Sanyal [a] *Semih Ener,*[b] *Evangelia Anagnostopoulou,* [a] *Marc Pousthomis,*[a] *Pier-Francesco Fazzini,*[a] *Lise-Marie Lacroix,*[a] *Konstantin P. Skokov,*[b] *Oliver Gutfleisch,*[b] *and Guillaume Viau* [a,]*

[a] Université de Toulouse, Laboratoire de Physique et Chimie des Nano-Objets, UMR 5215 INSA, CNRS, UPS, 135 avenue de Rangueil, F-31077 Toulouse cedex 4, France
[b] Funktionale Materialien, Institut für Materialwissenschaft, TU Darmstadt, 64287 Darmstadt, Germany

ABSTRACT

Core-shell magnetic anisotropic particles were prepared by reduction of Sb acetate at the surface of cobalt nanorods dispersed in a solution consisting of 1,2 tetradecanediol in oleylamine. X-ray diffraction and local EDS analyses revealed a thin β-CoSb shell with a controlled thickness ranging from 5 to 15 nm that depended on the Sb/Co molar ratio and the reduction temperature. The shell completely coats the rod surface but does not alter the shape anisotropy or the hcp structure of the cobalt cores, and the hard magnetic properties are preserved after coating with a coercivity higher than 3 kOe. Consolidated nanostructured materials that exhibit properties of permanent magnets were prepared by compaction of the core-shell Co@CoSb nanorods. The thin CoSb shell was very efficient for preventing the cobalt anisotropic core from sintering at high temperatures (up to 300°C) and high pressures (up to 1.5 GPa). These results indicate that the bottom-up approach is very promising for preparation of nanostructured hard magnetic materials.

TABLE OF CONTENT GRAPHIC

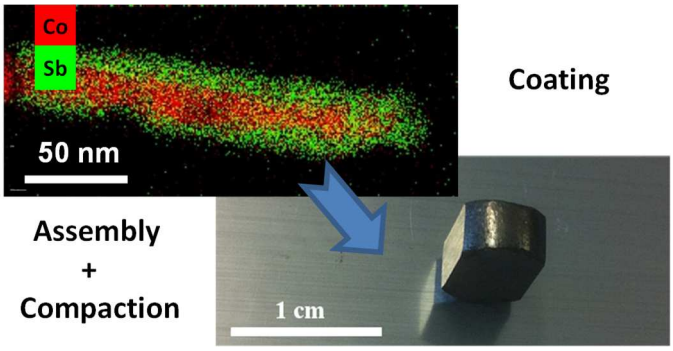

INTRODUCTION

The tremendous progress in liquid-phase synthesis has yielded metallic nanoparticles with controlled sizes and shapes, including nanoparticles prepared from iron-group transition metals, such as Fe, Co or Ni that exhibit unique magnetic properties due to their size reduction compared to the bulk materials. These promising materials could be used in data recording,[1] sensing or biomedical applications.[2] The synthesis of monometallic, alloy and oxide, magnetic nanoparticles being now well mastered, the focus has shifted to increasing the complexity by combining other properties, such as luminescence, plasmonic, catalytic activity, thermal stability or resistance, to oxidation within a single magnetic particle.[3] The synthesis of hybrid particles composed of different materials has been recently reviewed.[4,5] The overgrowth of a second material onto a predefined object is rather complex and leads to core-shell,[6] heterodimer[7] or dumbbell-like particles.[8]

Currently, most of the studies have focused on isotropic particles, and only a few studies have mention complex anisotropic objects. However, shape anisotropy is mandatory for several applications, such as plasmonic-based biodetection,[9] surface-specific catalytic reactions[10] or hard magnetic materials.[11] Recently, several groups have worked on the bottom-up approach of permanent magnets prepared with magnetic nanorods and nanowires.[12,13,14,15] Permanent magnets are a special class of magnetic material that exhibits both high coercivity and high magnetization. [16,17] In particular, cobalt nanorods (Co NRs) with a hcp structure are interesting for this application because when their long axis is parallel to the hcp c axis, they exhibit both shape and magnetocrystalline anisotropies. In this case, their magnetization loop exhibits a very high coercivity.[12] Different models have predicted that magnets consisting of Co NR assemblies that are sufficiently dense (magnetic volume fraction of c.a. 50%) to exhibit a high magnetization can achieve a high energy product, which is the figure of merit of a permanent magnet.[18,19] The interest in this new class of materials is their potential to fill the gap between hexaferrite- and rare earth-based permanent magnets.[13] Fabrication of Co NR-based magnets requires a compaction step to endow the rod assembly with mechanical strength. High coercivity in these materials could be obtained only when the magnetization reversal proceeds via individual reversal in each nanorods. Indeed, the small rod diameter makes difficult the nucleation of the magnetization reversal.[20,21] Therefore, two contradictory issues must be addressed by the compaction, a high cobalt NR volume fraction must be attained but at the same time the NR morphology must not be altered. For an increase in the

particle mean size and/or loss of shape anisotropy, the coercivity decreases substantially, preventing permanent magnet applications.[15]

Based on the results of previous studies, it is established that raw Co NRs undergo sintering and oxidation when they are heated at a temperature higher than 200°C.[22] Consolidation at the high pressures involved in the cold and hot compaction processes can produce the same effect. The growth of a thin layer at the Co NR surface could improve their stability. For example, encapsulation of the Co NRs in a thin carbon layer via treatment in organic solvents at a high temperature enhanced their thermal stability.[23] For the compaction process, an inorganic material is more favorable than a carbon shell but the growth of a continuous shell surrounding the Co NRs is not straightforward. Soulantica et al. studied the overgrowth of various metals on the Co NRs surface. Fe-Co dumbbells were formed by the growth of iron cubes at the cobalt NRs tips.[24] Co NRs decorated with gold nanoparticles were obtained by the overgrowth of gold,[25] but when the surface wettability was changed by adding trace amounts of Sn and Pt a continuous gold shell around the Co NRs was formed.[26]

In this study, we report the synthesis of original anisotropic core-shell Co@CoSb nanorods by growing a polycrystalline CoSb shell on the surface of pre-formed Co nanorods. Transition metal antimonides are intermetallic compounds that have attracted much interest due to their electric and thermoelectric[27,28,29] properties . Some antimonides have also been identified as interesting materials for use as anodes in lithium ion batteries.[30,31,32] However, the synthesis of metal antimonide nanoparticles has been rarely reported. Recently, Tremel et al. synthesized a series of nanocrystalline metal antimonides (M-Sb, M = Co, Ni, Fe, Cu_2, Zn) using metal complexes and Sb nanoparticles.[33,34] In addition, Schaak and co-workers described the formation of intermetallic compound using the polyol process,[35] and in particular, cobalt antimonide $CoSb_x$ (x=1, 3) nanocrystals were synthesized.[36] Herein, the reduction conditions to form CoSb nanoparticles from a mixture of cobalt and antimony precursors in oleylamine are reported, and we describe the structural and chemical characterization of the Co@CoSb nanorods obtained by reduction of antimony acetate at the surface of Co NRs prepared by the polyol process. A significant improvement in the high temperature stability of these materials was obtained compared to the raw cobalt rods. In addition, we report examples of consolidation on the core-shell Co@CoSb nanorods, demonstrating that dense materials can be obtained without altering the coercivity.

EXPERIMENTAL SECTION

Cobalt(II) acetate and antimony(III) acetate were purchased from Alfa Aesar, sodium hydroxide, lauric acid, 1,2-butanediol and oleylamine were obtained from Acros, and 1,2 tetradecanediol and hydrated ruthenium chloride were obtained from Sigma-Aldrich (ref. Sigma Aldrich 84050). All the raw chemicals were used without additional purification.

Preparation of Co nanorods: Cobalt nanowires were produced by the polyol process according to a previously reported procedure.[37] Cobalt laurate was prepared by mixing equimolar aqueous solutions of cobalt acetate and sodium laurate. The pink precipitate was washed with deionized water and dried overnight at 50°C to remove the excess water. The cobalt nanorods were prepared by reduction of cobalt laurate in a basic solution of 1,2-butanediol. A suspension of cobalt(II) laurate (8×10^{-2} mol.L^{-1}) was dispersed in a solution containing sodium hydroxide (7.5×10^{-2} mol.L^{-1}) in 1,2-butanediol. Ruthenium chloride was added to the medium to control the nucleation step ([Ru]/[Co] = 2.5%). The suspension was heated to 175°C for 30 min under mechanical stirring (speed 80 rpm). The solution turned black, indicating cobalt reduction. Then, the cobalt suspension was cooled to room temperature.

***Preparation of Co@CoSb nanorods*:** 10 mL of a suspension of Co nanorods in 1,2-butanediol (0.08 mol.L^{-1}) were taken, and the Co powder was isolated after washing several times with chloroform and absolute ethanol. Then, the resulting Co powder was transferred into a three-neck round-bottom flask containing 20 mL of oleylamine with the appropriate amounts of antimony acetate, $Sb(CH_3CO_2)_3$, and 1,2 tetradecanediol (TDD). The reaction mixture was heated to 250°C for 30 min. Next, the black-brown mixture was cooled to room temperature. Absolute ethanol was added at room temperature, and a black material was precipitated and isolated by centrifugation (10000 rpm). Then, the black powder was isolated after several washing with absolute ethanol.

In all experiments, the Co amount remained constant (0.8 mmol), and the Sb:TDD molar ratio was 3. Three Sb:Co compositions were targeted by varying the Sb amount.

Sample CoSb_8 (Sb:Co = 0.125): 29.9 mg (0.1 mmol) of antimony acetate, $Sb(CH_3CO_2)_3$ and 69.1 mg (0.3 mmol) of 1,2 tetradecanediol were added to 0.8 mmol of Co nanorods dispersed in oleylamine.

Sample CoSb_4 (Sb:Co = 0.25): 59.8 mg (0.2 mmol) of $Sb(CH_3CO_2)_2$ and 138.2 mg (0.6 mmol) of 1,2 tetradecanediol were introduced for the reaction.

Sample CoSb_2 (Sb:Co = 0.5): 119.6 mg (0.4 mmol) of $Sb(CH_3CO_2)_2$ and 276.4 mg (1.2 mmol) of 1,2 tetradecanediol were introduced for the reaction.

Preparation CoSb nanoparticles: In a typical experiment, 35.7 mg (0.1 mmol) of $Co(acac)_3$ and 28.9 mg (0.1 mmol) of $Sb(CH_3CO_2)_3$ were added to 20 mL of oleylamine and stirred vigorously until all the reagents were completely dissolved. The color of the solution became dark green. Then, the reaction was heated at 250°C for 30 min, which resulted a black colloid. The reaction mixture was allowed to cool at room temperature, and ethanol was added to this mixture. The black powder was precipitated, washed several times with absolute ethanol, collected by centrifugation and dried under air prior to characterization. In a second synthesis, 69.1 mg (0.3 mmol) of 1,2 tetradecanediol was added to the starting mixture.

Annealing experiments: To carry out the annealing experiment, the Co@CoSb powders were placed in a ceramic boat and transferred into a furnace. The annealing experiment was carried out under forming gas (i.e., Ar + H_2 (7%)) for 1 h at various temperatures (i.e., 250°C, 300°C and 400°C). Then, the powders were allowed to cool to room temperature under Ar gas and used for further characterization.

Consolidation: The Co@CoSb nanorods were consolidated into bulk materials to investigate the possibility of preparing bulk permanent magnets. The consolidation studies were carried out in two different ways involving cold compaction and hot pressing. For cold compaction, a uniaxial hydraulic press that was equipped with a 1.7 T electromagnet was used. The direction of the magnetic field was perpendicular to the pressing direction. In addition, an electromagnet was used to create “green bodies (pre-aligned nanorods)”, which were used for hot compaction. The measured densities of the consolidated materials were calculated from their weight and volume. The theoretical densities were calculated according to the Co@CoSb chemical compositions, and possible organic compounds were neglected. The packing densities were calculated from the ratios of the measured and theoretical densities of the samples. Hot compaction of the green bodies was performed at 180°C under a pressure of 150 MPa for 2 min.

Characterization: The transmission electron microscopy (TEM) characterizations were performed using a JEOL 1400 microscope operating at 120 kV. High-resolution transmission electron microscopy (HRTEM) images and scanning transmission electron microscopy (STEM) - energy dispersive X-ray (EDX) mapping were acquired on a JEOL 2100F field emission transmission electron microscope that operated at 200 kV. To prepare the TEM

samples, the metal nanopowder was redispersed in chloroform by sonication for approximately, 15 min and then, 2 μL of this suspension was placed on a carbon-coated copper grid and dried under vacuum. The X-ray diffraction measurements were carried out using a PANalytical X'Pert Pro diffractometer that was equipped with an X'celerator detector using Co K_α radiation (λ = 1.7889 Å). All the measurements were carried out in a 2θ range of 25-85° with a 0.067° step size and 300 s per step. The magnetic properties of the powders of randomly oriented core-shell Co@CoSb nanorods were investigated up to 3T using a Quantum Design Physical Property Measurement System (PPMS) with a vibrating sample magnetometer (VSM) configuration. The magnetic characterizations of the compacted samples were performed with a Metis pulse magnetometer. The demagnetization corrections were performed using the shape and dimensions of the consolidated products. Full hysteresis measurements were performed in an external field interval of -3.6 to -3.6 T. The magnetic measurements of the bulk magnets were performed with the applied field parallel to the direction of the magnetic field used for rod alignment during (CP) or before (HP) consolidation.

RESULTS AND DISCUSSION

Formation of CoSb alloy nanostructures. The powders prepared by the reaction of 5 mM of $Co(acac)_3$ and 5 mM of $Sb(CH_3CO_2)_3$ in hot oleylamine were analyzed by TEM and X-ray diffraction (XRD). When the reaction mixture was heated to 250°C for 30 min, the XRD pattern of the final powder exhibited peaks corresponding to the β-CoSb alloy[38] with a NiAs structure (jcpds file n° 33-0097) along with peaks that were assigned to antimony oxide (Sb_2O_3, jcpds file n° 05-0534) (Fig. 1). When the same reaction was carried out in the presence of 1,2 tetradecanediol (15 mM), the powder XRD pattern exhibited only reflections corresponding to CoSb, demonstrating that the formation of antimony oxide was completely inhibited (Fig. 1). The TEM images showed agglomerated nanoplatelets (supplementary information, Fig. S1). Reduction of $Co(acac)_3$ in oleylamine has been previously employed to produced small Co nanoparticles.[39] Here, we demonstrated that hot oleylamine can also reduce antimony acetate. However, to avoid antimony oxide formation, the addition of tetradecanediol was required. The effect of tetradecanediol can be interpreted in two ways. First, TDD may be a stronger reducing agent than oleylamine, and second, as an α-diol, TDD may form an alkoxide at high temperatures with the Sb^{3+} cations, preventing the formation of Sb oxide. Interestingly, phase separation leading to pure Sb and Co NPs did not occur, and

the binary CoSb alloy was easily obtained. Kieslich *et al.* previously demonstrated that the thermodecomposition of $Co_2(CO)_8$ at 280°C in the presence of Sb nanoparticles leads to binary CoSb particles.[33] We confirmed that Co and Sb easily form alloys using a high-temperature liquid-phase process.

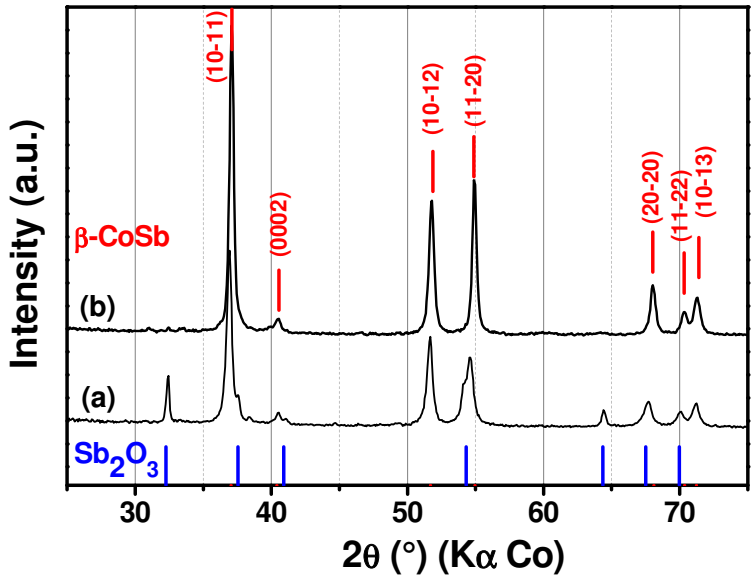

Figure 1. XRD pattern of powders prepared by reaction of an equimolar mixture of $Co(acac)_3$ (5 mM) and $Sb(CH_3CO_2)_3$ (5 mM) in oleylamine at 250°C for 30 min (a) in the absence of TDD and (b) in the presence of TDD (15 mM).

Co@CoSb nanorod synthesis via reaction of antimony acetate with Co NRs

Effect of the reaction temperature

Based on our results obtained for the synthesis of CoSb nanoparticles, we investigated coating anisotropic Co nanorods with a CoSb shell using TDD as a reducing agent. To favor the heterogeneous growth of Sb at the surface of the Co NRs and prevent self-nucleation, we lowered the reaction temperature and used a Sb/Co ratio of 1/4 and a reaction time of 30 min. At 150°C, Sb_2O_3 nanoparticles precipitated next to the hcp Co nanorods, as shown by the TEM image and XRD pattern (Fig. 2a,d). This result suggests that this temperature allows for nucleation of Sb_2O_3 nanoparticles but is not sufficient to reduce the Sb(III) species. At 200°C, the Co nanorods appeared to evolve, and darker contrast and cubic facets were observed in the TEM image (Fig. 2b). Small particles were still observed. The formation of

the β-CoSb alloy at the surface of the Co rods was confirmed by XRD. Extending the reaction time to 2 h leads to the disappearance of Sb_2O_3 along with an increasing formation of the CoSb alloy (Fig. 2d). The modification of the Co rod surface was observed in the TEM image (Fig. 2c).

These results suggest that the growth of the CoSb shell at the surface of the Co rods proceeded through a two-step process as follows: i) nucleation of Sb_2O_3 particles in solution followed by ii) their redissolution and reduction of Sb(III) species to form the CoSb alloy at the rod surface.

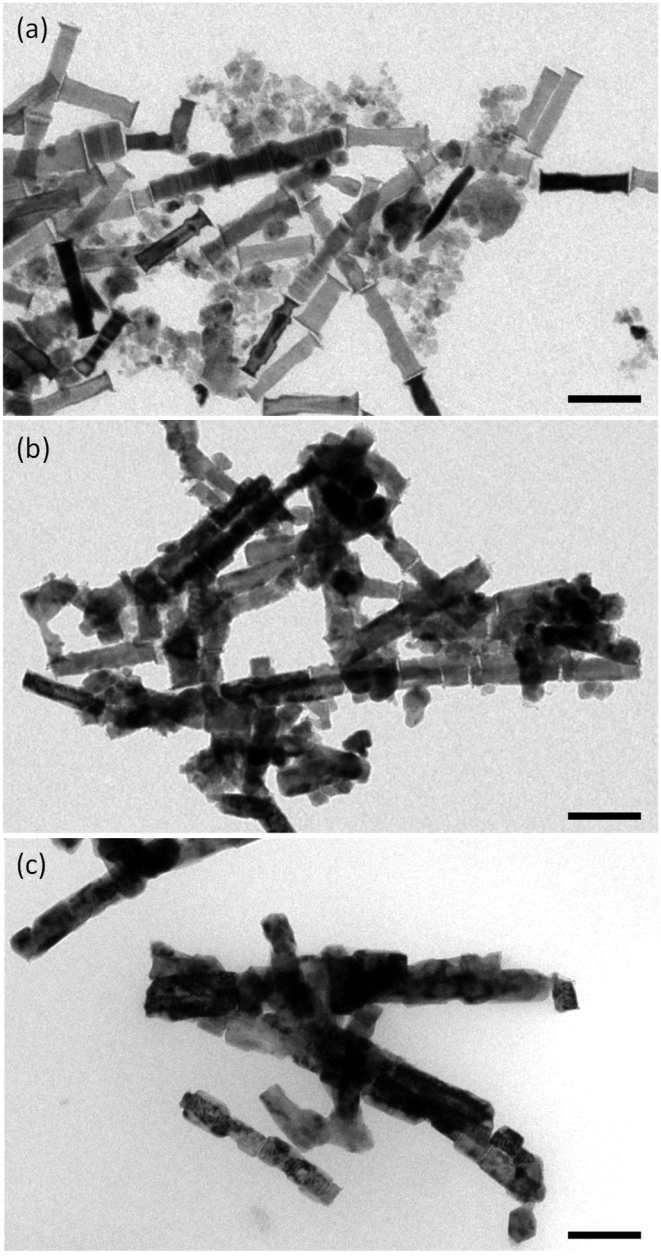

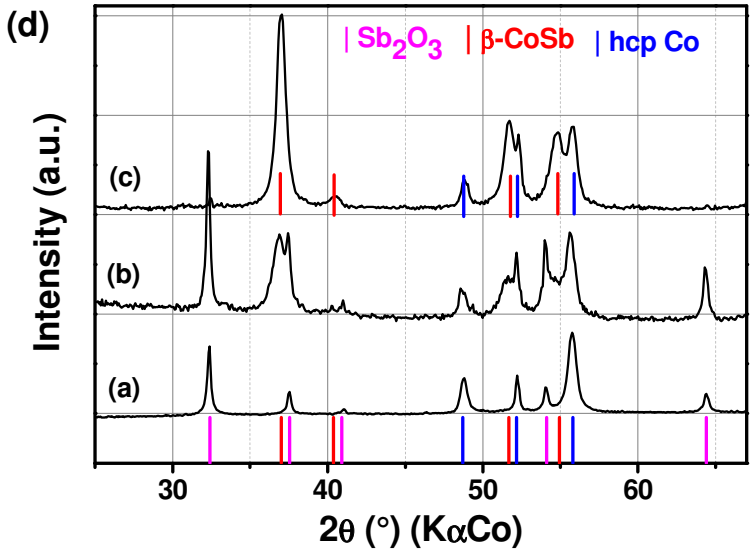

Figure 2. (a-c) TEM images of the particles obtained by reaction of antimony(III) acetate with Co nanorods in oleylamine at (a) 150°C for 30 min, (b) 200°C for 30 min, and (c) 200°C for 2 h (Sb/Co atomic ratio of 1/4). The scale bars represent 100 nm. (d) X-ray diffraction pattern of powders from (a), (b) and (c).

Effect of the Sb/Co ratio

To increase the rate of the reaction and ensure total reduction of the Sb(III) species, the reaction conditions were chosen to be 250°C for 30 min. The TEM images and XRD patterns of the powders synthesized with Sb/Co molar ratios varying between 1/8 and 1/2 are shown in figure 3. Under these conditions, the precipitation of Sb_2O_3 particles was not observed, which was confirmed by XRD and TEM analyses. The TEM images indicated the preservation of the anisotropic morphology of the nanoparticles regardless of the Sb amount added to the reaction. For low Sb/Co ratios ($\leq$ 1/4), the coating is fairly inhomogeneous, and completely covered rods as well as naked rods can be observed. In addition, intermediate states consisting of small islands were observed at the Co NR surface (Fig. 3a-b). An Sb/Co ratio of 1/2 was required to obtain completely covered rods embedded in a continuous CoSb shell. The XRD patterns were indexed as a mixture of hcp Co and CoSb, and the relative intensity of the CoSb peaks increased with the initial Sb/Co ratio (Fig. 3d). For a coating with a Sb/Co ratio of 1/4, comparison of figures 2c and 3b indicates that a more homogeneous coating was achieved when the reaction was carried out at a lower temperature.

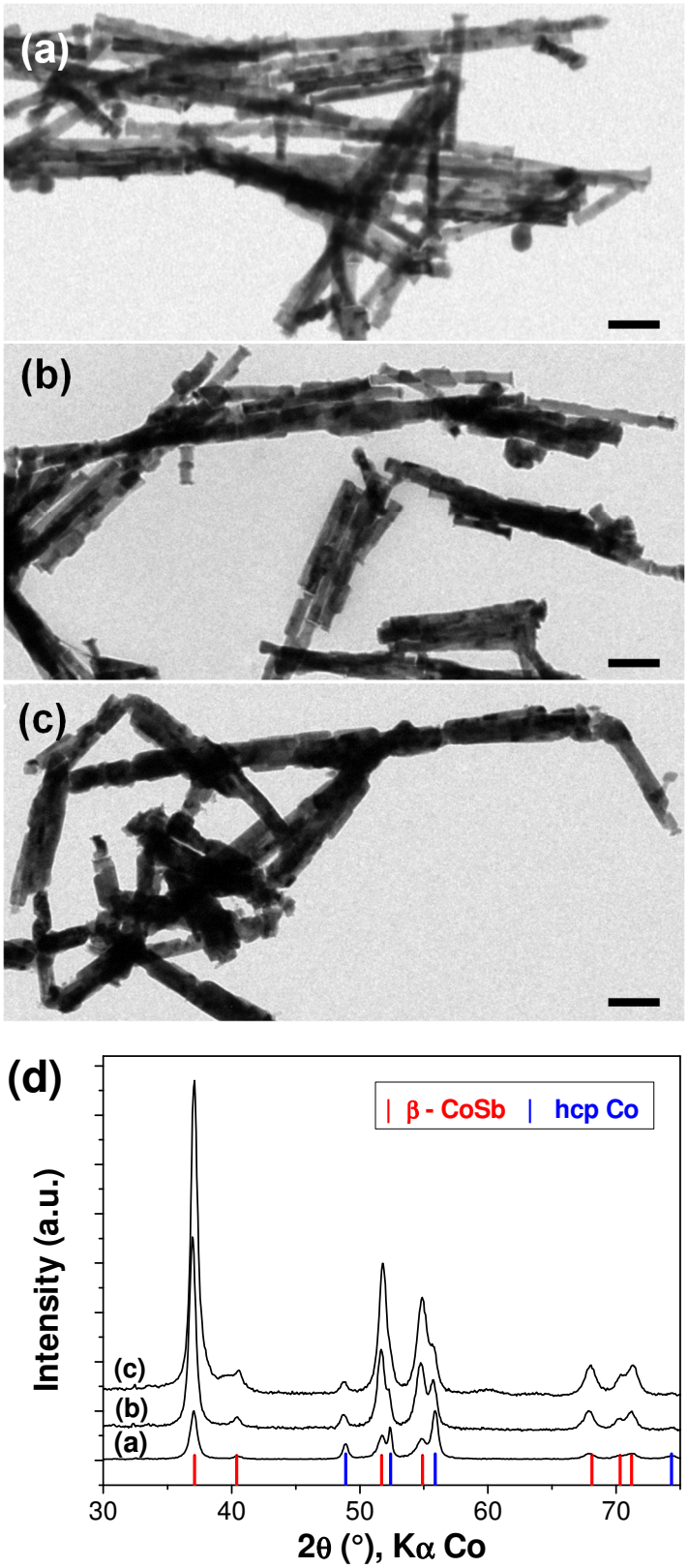

Figure 3. (a-c) TEM images of the particles obtained by reaction of antimony(III) acetate with Co nanorods in oleylamine at 250°C for 30 min with various Sb/Co atomic ratios: (a)

Sb/Co = 1/8, (b) Sb/Co = 1/4, and (c) Sb/Co = 1/2. The scale bars represent 100 nm. (d) X-ray diffraction pattern.

Chemical analysis

The Sb and Co contents in the final powder were determined based on energy dispersive X-ray analysis on large areas that was measured with scanning electron microscopy. The Sb/Co ratio in the final powder was always 1.5 times higher than that in the starting mixture (Tab. 1, and Fig. S2 of supplementary materials). This observation suggests partial dissolution of the cobalt rods concomitantly with CoSb alloy growth. Local EDS analysis was performed using scanning transmission electron microscopy (STEM-EDS) to confirm the chemical composition in the core and shell regions of the Co@CoSb rods.

Figure 4 shows the HAADF images of the Co/CoSb nanorods and the corresponding Co, Sb, and combined chemical mappings inferred from STEM-EDS analysis. A core-shell microstructure was confirmed by the maximum intensity of the Co content being located in the center of the rod and the Sb content being located on the edge. The shell appeared nearly continuous around the inner cobalt rod, and its thickness increased when the Sb amount in the reaction increased. The presence of an inner Co core and a shell consisting of a stoichiometric CoSb alloy was confirmed by local EDS analysis. Figure 4m shows the emission spectra obtained from the center and edge of a Co/CoSb nanorod prepared with a Sb/Co ratio of 1/2. The corresponding Co-Sb compositions were determined to be $Co_{75}Sb_{25}$ at the center and $Co_{55}Sb_{45}$ at the edge, showing that the edge composition was very close to the stoichiometry of the intermetallic compound expected from the XRD pattern. As the core-shell texture was established, the chemical composition of the Co/CoSb samples is given as $Co_x@(Co_{0.5}Sb_{0.5})_y$ in table 1. For the same parent Co NRs, we followed the variation in the internal Co rod diameter (d_{Co}) and the CoSb shell thickness (e_{CoSb}) as a function of the Sb/Co ratio. When the Sb/Co ratio varied from 1/8 to 1/2, d_{Co} decreased from 22 to 14 nm, and e_{CoSb} increased from 5 to 15 nm (Tab. 1).

Table 1. Chemical composition and mean diameter (d_{total}) of the Co/CoSb samples prepared by reaction of antimony(III) acetate with Co nanorods in oleylamine at 250°C for 30 min with various Sb/Co atomic ratios. The diameter of the inner core (d_{Co}) and the thickness of the CoSb shell (e_{CoSb}), which were determined from STEM-EDS analysis, are also listed.

Samples	**Global compo. (at. %)**		**Core-Shell compo. (at. %)**	d_{Co}	$\mathbf{e_{CoSb}}$	d_{total}
	Targeted	Measured	$\mathbf{Co_x@(Co_{0.5}Sb_{0.5})_y}$	**(nm)**	**(nm)**	**(nm)**
Sb/Co = 1/8	$Co_{89}Sb_{11}$	$Co_{85}Sb_{15}$	$\mathbf{Co_{70}@(Co_{0.5}Sb_{0.5})_{30}}$	22	5	32
Sb/Co = 1/4	$Co_{80}Sb_{20}$	$Co_{75}Sb_{25}$	$\mathbf{Co_{50}@(Co_{0.5}Sb_{0.5})_{50}}$	18	8	34
Sb/Co = 1/2	$Co_{67}Sb_{33}$	$Co_{57}Sb_{43}$	$\mathbf{Co_{14}@(Co_{0.5}Sb_{0.5})_{86}}$	14	15	44

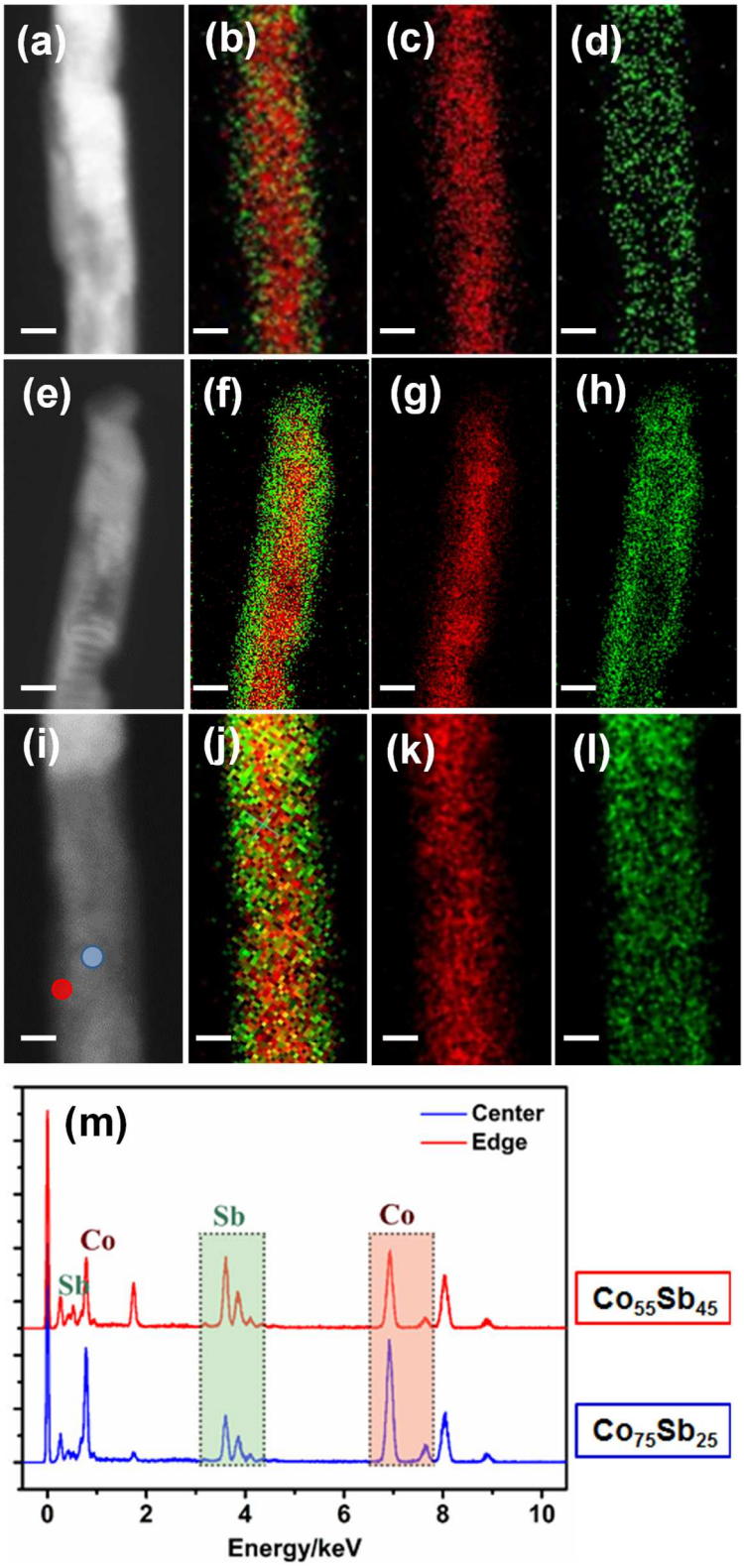

Figure 4. STEM-HAADF images and EDS chemical mapping of the Co@CoSb particles prepared by reaction of Sb^{III}acetate with Co NRs: (a)-(d) Sb/Co ratio = 1/8, (e)-(h) Sb/Co ratio = 1/4, and (i)-(l) Sb/Co ratio = 1/2. The scale bar represents 20 nm. (m) EDS spectra recorded at the center and on the edge of a single Co@CoSb rod (Sb/Co ratio = 1/2).

Microstructure

XRD line broadening can provide microstructural information that is averaged over billions of particles. For the Co NRs prepared by the polyol process, the XRD line broadening is strongly dependent on the (hkil) indexes. The (0002) line is always much narrower than the (10-10) line, which demonstrates a crystallographic coherence that is higher along the c axis than perpendicular to the c axis. This characteristic indicates that the rod growth axis is parallel to the crystallographic c axis.[37,40] To follow the variation in the mean crystallite size of the hcp-Co core and the ß-CoSb shell, the XRD patterns of the Co@CoSb rods were fitted using pseudo-Voight profiles (Fig. 4a). The crystallite sizes for different lines of the hcp-Co and ß-CoSb phases of the Co@CoSb pattern as a function of increasing Sb content are plotted in figure 4b. The mean crystallite size (L(0002)) calculated from the (0002) line broadening was higher than the crystallite size (L(10-10)) calculated from the (10-10) line broadening. This observation confirms that the shape anisotropy of the parent Co NRs was preserved after CoSb coating. For the CoSb shell, no clear anisotropy of the crystallites was detected. The mean crystallite sizes calculated for the first three more intense reflections (i.e., (10-11), (10-12) and (11-20)) of the ß-CoSb phase were very close (i.e., in the range 13-20 nm). Therefore, the CoSb shell was polycrystalline, and an epitaxial relationship between CoSb and the parent Co rod was not observed.

Figure 6 shows a high-resolution electron microscopy image of a Co@CoSb NR prepared with a Sb/Co ratio of 1/4. A lattice fringe spacing that corresponds to the CoSb {hkil} planes was observed. The CoSb shell was polycrystalline with two different crystallographic orientations based on the numerical diffraction patterns. Figure S3 (see supplementary materials) shows two additional examples of HRTEM images for Co@CoSb NRs prepared under the same conditions. The lattice fringes corresponding to the CoSb {10-11} planes were observed in both cases that spread across the entire area. However, their orientations with respect to the rod axis were different, confirming the polycrystallinity of the CoSb shell. The analysis of HRTEM images of Co@CoSb with a thicker shell, which was prepared with a Sb/Co ratio of 1/2, was difficult due to the superposition of the CoSb crystals in a different zone axis.

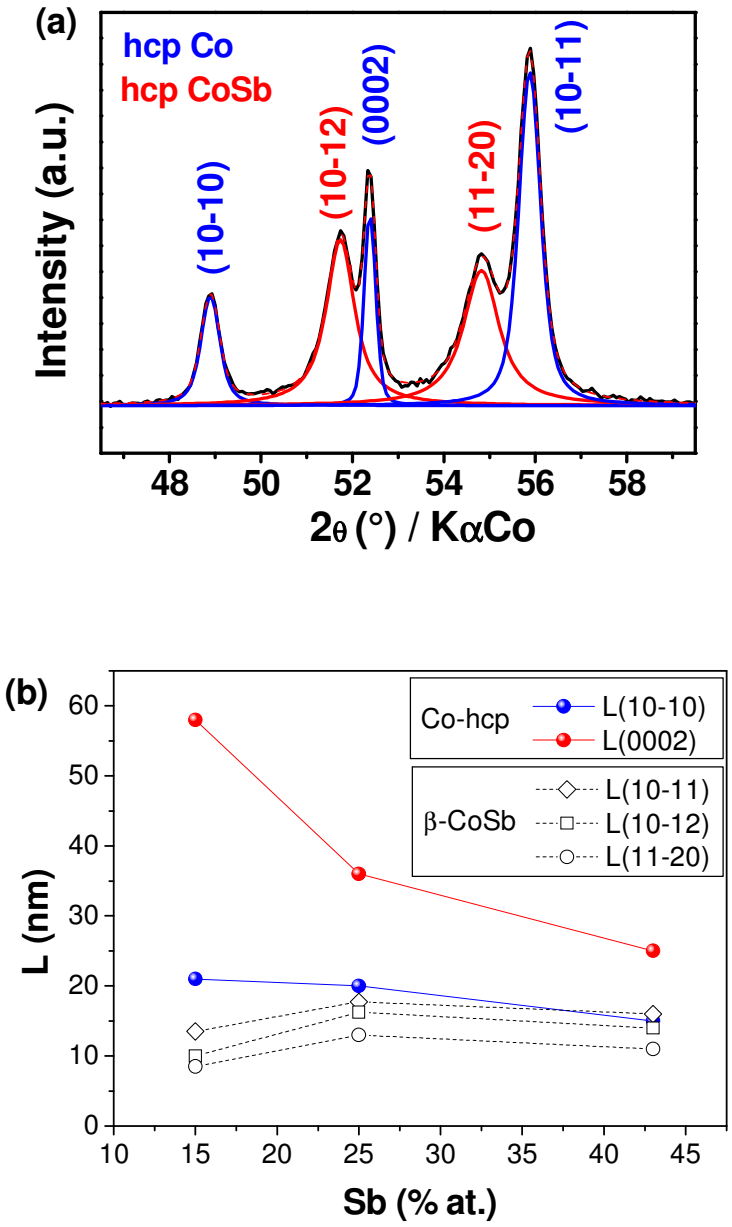

Figure 5. (a) Line analysis of the XRD pattern of the $Co_{70}@(Co_{0,5}Sb_{0.5})_{30}$ nanorods in a 2θ range of 45-60°. (b) Evolution of the (0002) and (10-10) crystallite sizes of the hcp Co and (10-11), (10-12) and (11-20) crystallite sizes of the β-CoSb as a function of the Sb content.

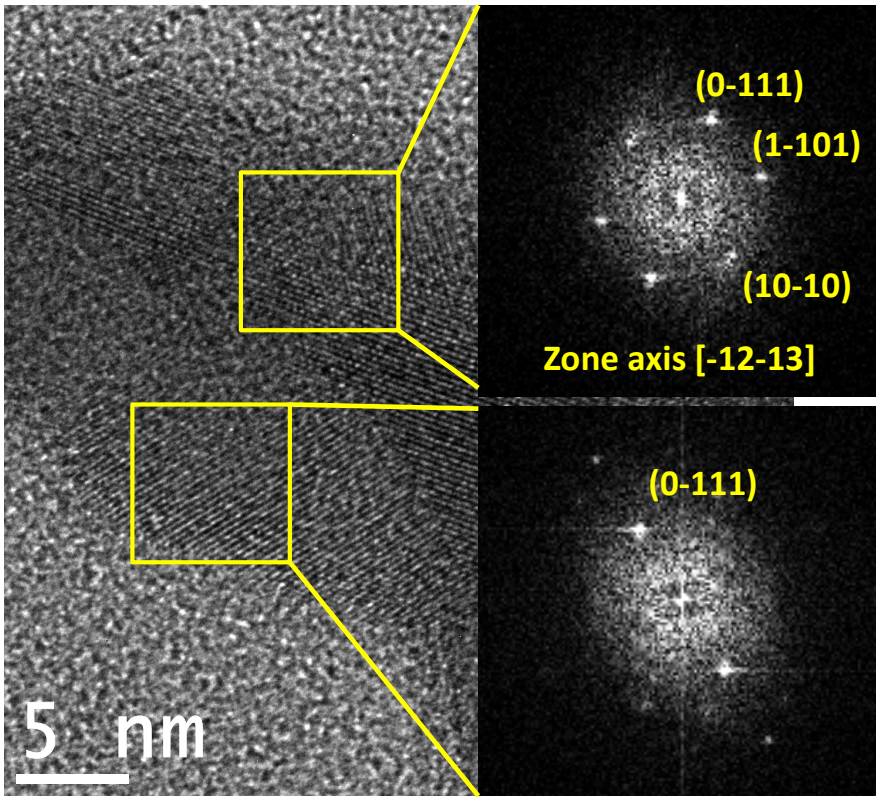

Figure 6. HRTEM image of a Co@CoSb rod prepared with a Sb/Co ratio of 1/4 and a numerical diffraction pattern calculated on the two square zones showing two different crystallographic orientations.

Thermal stability and magnetic properties of the Co@CoSb nanorods. To investigate the high-temperature stability of the Co@CoSb nanorods, annealing from 250°C to 400°C under forming gas was carried out for 1 h. Figure S4 in the supplementary information shows the room temperature XRD patterns of the $Co_{50}@(Co_{0.5}Sb_{0.5})_{50}$ powders that were obtained after annealing at various temperatures. No apparent change was observed, and the reflections due to both hcp Co and CoSb were observed without any variation in the relative intensities. No additional phase appeared even after annealing at 400°C. The same observation was performed for the other Co@CoSb compositions. The effect of annealing on the morphology of the Co@CoSb nanorods was studied by TEM (Fig. S5 of supplementary information). Although no significant difference was observed between the raw Co@CoSb particles and those annealed at 300°C, the particles appeared to be more agglomerated after annealing at 400°C. However, their anisotropic morphology appears to be preserved. Therefore, 400°C is

most likely the onset temperature of sintering of the CoSb alloy, leading to the coalescence of nanorods.

The texture of the Co hcp phase was examined in more detail to follow any variation in the anisotropy of the Co cores. The crystallite sizes calculated from the (10-10), (0002) and (10-11) line broadening in the $Co_{50}@(Co_{0.5}Sb_{0.5})_{50}$ sample that was annealed at different temperatures are shown in figure 7. The corresponding XRD patterns are provided in the supplementary information (Fig. S7). The crystallite sizes of the Co hcp phase were nearly constant (Fig. 7), confirming that the anisotropy of the Co cores was preserved during annealing even up to 400°C. The crystallite size of the β-CoSb phase increased only slightly due to annealing at 300°C (Fig. 7). After annealing at 400°C, the crystallite sizes doubled (Fig. 7), indicating strong modification of the shell texture that is in agreement with the coalescence observed in the TEM images (Fig. S5). The same trends were observed for the $Co_{70}@(Co_{0.5}Sb_{0.5})_{30}$ powders (see supplementary information Fig. S7 and S8).

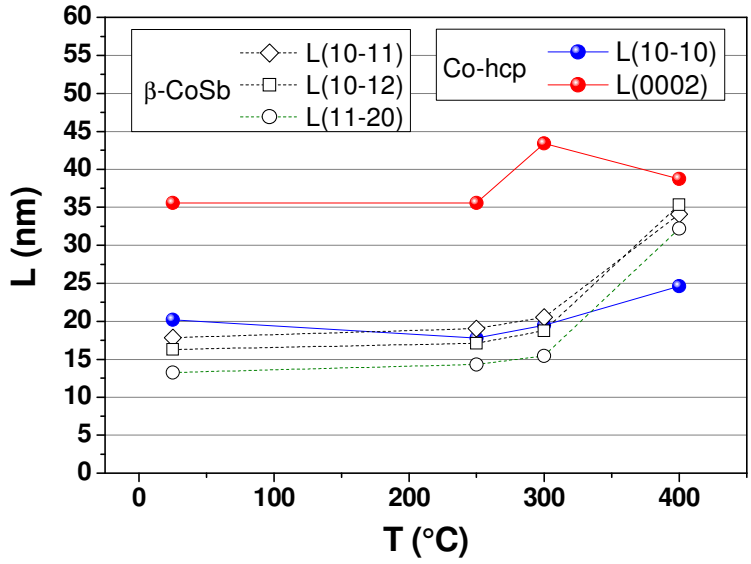

Figure 7. Crystallite size of the $Co_{50}@(Co_{0.5}Sb_{0.5})_{50}$ particles measured after annealing under forming gas at different temperature for the Co hcp phase perpendicular and parallel to the *c* axis calculated from the (10-10) and (0002) line broadening, respectively, and for the (10-11), (10-12) and (11-20) reflections of the β-CoSb phase. The fit of the corresponding XRD patterns is provides in the supplementary materials (Fig. S6).

The room temperature magnetization loops M(H) for different Co@CoSb powders that were annealed under forming gas are shown in figure 8. In each case, the remanence to saturation ratio was 0.5, which is the value expected for a randomly oriented anisotropic particle assembly. The coercivity of the Co NRs depends on their aspect ratio and crystallinity.[20] The coercivities of the parent Co NRs and the Co@CoSb powders were 3.1 kOe and 3.1 – 3.4 kOe, respectively (Table 2). Therefore, the Co NR coating with CoSb did not alter the coercivity. The magnetic measurement confirmed that the anisotropy of the hcp Co core was preserved during the coating and annealing processes. Therefore, surface modification of the Co nanorods with CoSb enhanced their thermal stability. A similar annealing experiment was performed on the uncoated Co nanorods and indicated that they were stable only up to 200°C (the anisotropic structure is lost above this temperature).[22]

The spontaneous magnetization per gram of sample (M_s) decreased as the CoSb content in the Co@CoSb composition increased (Table 2). CoSb is a paramagnetic compound,[41] and only the ferromagnetic Co cores contribute to the magnetization at room temperature. The theoretical Ms of the Co@CoSb powders, which is expressed in emu.g^{-1}, was calculated as the product of the hcp Co weight percent and the bulk Co spontaneous magnetization (Ms(Co) = 160 emu.g^{-1}). The experimental values for the $Co_{70}@(CoSb)_{30}$ and $Co_{50}@(CoSb)_{50}$ samples were slightly lower than the expected values (78% and 84%, respectively). This result may be due to the presence of carbon at the surface of the particles due to a low annealing temperature, by minor diffusion of Co into the CoSb phase during the annealing process that could lower the magnetization, or by magnetic disorder at the Co/CoSb interface (spin canting).

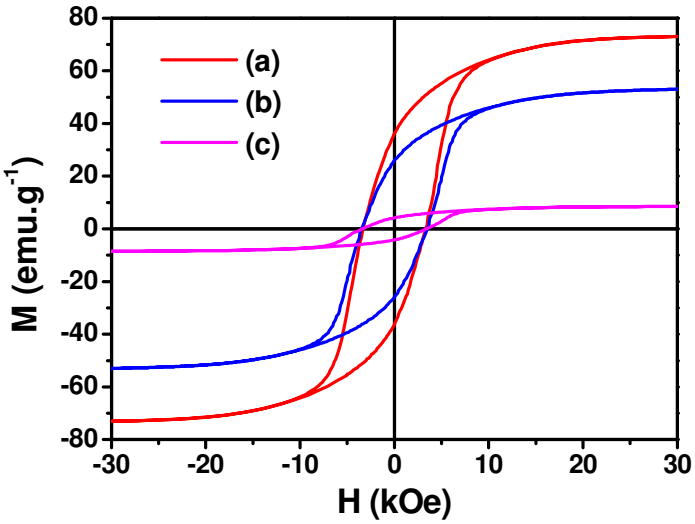

Figure 8. Room temperature magnetization loop of the Co@CoSb powders annealed under forming gas at 300°C: (a) $Co_{70}@(Co_{0.5}Sb_{0.5})_{30}$, (b) $Co_{50}@(Co_{0.5}Sb_{0.5})_{50}$, and (c) $Co_{14}@(Co_{0.5}Sb_{0.5})_{86}$.

Table 2. Room temperature coercivity and spontaneous magnetization of Co@CoSb powders after annealing at 300°C for 1 h under forming gas. The theoretical Ms was calculated as the product of the weight percent of hcp Co and the bulk Co magnetization.

Co@CoSb (at. %)	$Co_{70}@(CoSb)_{30}$	$Co_{50}@(CoSb)_{50}$	$Co_{14}@(CoSb)_{86}$
Co@CoSb (weight %)	$Co_{60.3}@(CoSb)_{39.7}$	$Co_{39.5}@(CoSb)_{60.5}$	$Co_{9.6}@(CoSb)_{90.4}$
Hc (kOe)	3.1	3.4	3.4
Ms($emu.g^{-1}$) exp. / theor.	75 / 96.5	53 / 63	8.5 / 15

Consolidation of the Co@CoSb nanorods. Bulk magnets were obtained by cold and hot consolidation of the $Co_{70}@(CoSb)_{30}$ nanorods (Fig. 9). Their properties are summarized in table 3. The cold-pressed sample exhibited the highest packing density (56%), which was induced by an applied pressure of 1.5 GPa. A lower pressure of 150 MPa was applied during the hot compaction, which results in a lower density (46%). The Co@CoSb nanorods tend to create agglomerates, and an applied external magnetic field of 1.7 T was not sufficiently strong to disentangle these agglomerates and create a perfect alignment. The M_r/M_s ratio was

higher in the hot-compacted sample (60%). The high pressure used for the cold-pressed sample disturbed the alignment of the nanorods and decreased the M_r/M_s ratio (46%). The coercivity of the two consolidated samples was equal to 3.1 kOe, which is the same as that measured for the $Co_{70}@(CoSb)_{30}$ nanorods prior to compaction (Tab. 2). Therefore, the cobalt core was preserved during cold compaction under 1.5 GPa and hot compaction at 180°C. The cobalt core sintering was avoided due to the thin CoSb shell. The compacted samples exhibited the properties of a permanent magnet, and figure 9 shows a sample strongly attached to a vertical steel plate. The energy product of the hot-compacted sample was equal to 10 $kJ.m^{-3}$. This value is lower than the energy product of aligned nanorods. An improvement in this value requires better alignment of the Co@CoSb rods to increase the Mr/Ms and the squareness of the magnetization curve.

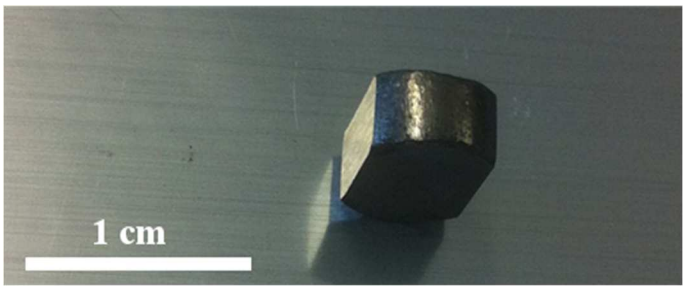

Figure 9. Bulk magnet obtained by hot compaction of $Co_{70}@(Co_{0.5}Sb_{0.5})_{30}$ nanorods (150 MPa, 180°C).

Table 3. Summary of consolidated samples of Co@CoSb nanorods: CP – cold pressed (compacted) and HP – Hot pressed (the magnetic field was parallel to the direction of the field used to align the rods during the compaction process)

Sample	$\rho_{Measured}$ (g/cm^3)	$\rho_{Theoretical}$ (g/cm^3)	Packing fraction (%)	M_r/M_s ratio (%)	Hc (kOe)
Co@CoSb - CP	4.844	8.66	56	46	3.1
Co@CoSb - HP	3.968	8.66	46	60	3.1

CONCLUSION

In this study, we have demonstrated that core-shell Co@CoSb anisotropic particles can be obtained by coating Co nanorods with a CoSb alloy in a one-pot reaction. Reduction of $Sb(CH_3CO_2)_3$ in a solution of oleylamine containing tetradecanediol and in the presence of Co NRs leads to the growth of a thin polycrystalline β-CoSb shell that progressively surrounds the entire rod with increasing time. The CoSb shell thickness can be varied based on the Sb amount introduced into the reaction. The CoSb growth at the surface of the rods occurs in a temperature range between 200 and 250°C and most likely involves the partial dissolution of the cobalt based on the chemical analysis. The shape and hcp Co crystal anisotropy of the parent rod are preserved after coating. Therefore, the coercivity of the Co@CoSb rods is similar to that of the parent Co rods. The CoSb coating enhanced the thermal stability of the Co NRs. Under forming gas, the shell acts as a barrier that prevents Co core agglomeration and preserves their shape anisotropy and magnetic properties. The consolidation studies demonstrated that macroscopic magnets can be prepared from the Co@CoSb nanorods. The magnetic measurements indicated that the integrity of the anisotropic cobalt core was preserved even after compaction at 1.5 GPa. The highest packing density was obtained for the cold-compacted samples where the highest pressure was applied. Nevertheless, our results indicate that to achieve the best magnetic properties, hot compaction should be used on pre-aligned nanorods. A higher packing density and higher degree of alignment of the nanorods are required to further improve the magnet performance.

ACKNOWLEDGEMENT

This work was supported by the European Commission for the REFREEPERMAG FP7 project (EU NMP3-SL-2012-280670).

ASSOCIATED CONTENT

Supporting Information for Publication in file cm-2016-01196c SI.pdf, including TEM images of CoSb NPs, EDX analysis results on Co@CoSb rods, complementary HRTEM images, TEM and XRD of Co@CoSb rods after annealing at different temperatures, M(H) loop of consolidated Co@CoSb magnet.

AUTHORS INFORMATION

Corresponding author

*E-mail: guillaume.viau@insa-toulouse.fr

REFERENCES

[1] Liakakos, N.; Blon, T.; Achkar, C.; Cormary, B. ; Ran, R. P.; Benamara, O.; Chaboussant, G.; Ott, F.; Warot-Fonrose, B.; Snoeck, E.; Chaudret, B.; Soulantica, K. and Respaud, M. Solution Epitaxial Growth of Cobalt Nanowires on Crystalline Substrates for Data Storage Densities beyond 1 Tbit/in2. *Nano Lett.* **2014**, *14*, 3481-3486.

[2] Lu, A.-H.; Salabas, E. L. and Schüth, F. Magnetic nanoparticles: synthesis, protection, functionalization, and application. *Angew. Chem. Int. Ed.* **2007**, *46*, 1222-1242.

[3] Salgueiriño-Maceira, V. and Correa-Duarte, M.A. Increasing the Complexity of Magnetic Core/Shell Structured Nanocomposites for Biological Applications. *Adv. Mater* **2007**, *19*, 4131-4144.

[4] Chaudhuri, R. B. and Paria S. Core/shell nanoparticles: classes, properties, synthesis mechanisms, characterization, and applications. *Chem. Rev.* **2012**, *112*, 2373-2433.

[5] Hao, R.; Xing, R. Xu, Z.; Hou, Y.; Gao, S. and Sun S. Synthesis, functionalization, and biomedical applications of multifunctional magnetic nanoparticles. *Adv. Mater.* **2010**, *22*, 2729-2742.

[6] Wei, S.; Wang, Q.; Zhu, J.; Sun, L.; Line, H. and Guo Z. Multifunctional composite core-shell nanoparticles. *Nanoscale* **2011**, *3*, 4474-4502.

[7] Cozzoli, P.D.; Pellegrino, T.; Manna L. Synthesis, properties and perspectives of hybrid nanocrystal structures. *Chem. Soc. Rev.* **2006**, *35*, 1195-1208.

[8] Wang, C.; Xu, C.; Zeng, H. and Sun S. Recent Progress in Syntheses and Applications of Dumbbell-like Nanoparticles. *Adv. Mater.* **2009**, *21*, 3045-3052.

[9] Schrittwieser, S.; Ludwig, F.; Dieckhoff, J.; Soulantica, K.; Viau, G.; Lacroix, L.-M.; Lentijo, S. M.; Boubekri, R.; Maynadié, J.; Huetten, A.; Brueckl, H. and Schotter, J. Modeling and Development of a Biosensor Based on Optical Relaxation Measurements of Hybrid Nanoparticles. *ACS Nano*, **2012**, *6*, 791-801.

[10] Liu, Q.Y. ; Cao, X.F.; Wang, T.J. ; Wang, C.G.; Zhang, Q.; Ma, L.L. Synthesis of shape-controllable cobalt nanoparticles and their shape-dependent performance in glycerol hydrogenolysis. *RSC Adv.* **2015**, *5*, 4861-4871.

[11] Maurer, T.; Ott, F.; Chaboussant, G.; Soumare, Y.; Piquemal, J.-Y.; Viau, G. Magnetic nanowires as permanent magnet materials. *Appl. Phys. Lett.* **2007**, *91*, 172501.

[12] Gandha, K.; Elkins, K.; Poudyal, N.; Liu, X.; Liu, J. P. High Energy Product Developed from Cobalt Nanowires. *Sci. Rep.* **2014**, *4*, 5345.

[13] Anagnostopoulou, L.; Grindi, B.; Lacroix, L.-M. ; Ott, F. ; Panagiotopoulos, I. and Viau, G. Dense arrays of cobalt nanorods as rare-earth free permanent magnets. *Nanoscale*, **2016**, *8*, 4020-4029.

[14] Liébana-Viñas, S.; Wiedwald, U.; Elsukova, A.; Perl, J.; Zingsem, B.; Semisalova, A. S.; Salgueiriño, V.; Spasova, M.; Farle, M. Structure-Correlated Exchange Anisotropy in Oxidized $Co_{80}Ni_{20}$ Nanorods. *Chem. Mater.* **2015**, *27*, 4015-4022.

[15] Ouar, N.; Bousnina, M. A.; Schoenstein, F.; Mercone, S.; Brinza, O.; Farhat,S.; Jouini, N. Spark Plasma Sintering of $Co_{80}Ni_{20}$ nanopowders synthesized by polyol process and their magnetic and mechanical properties. *J. Alloys Compd* **2014**, *615*, S269–S275.

[16] Gutfleisch, O.; Willard, M. A.; Brück, E.; Chen, C. H.; Sankar, S. G.; Liu, J. P. Magnetic Materials and Devices for the 21st Century: Stronger, Lighter, and More Energy Efficient. *Adv. Mater.* **2011**, *23*, 821-842.

[17] Gutfleisch, O. Controlling the properties of high density permanent magnetic materials. *J. Phys. D: Appl. Phys.* **2000**, *33*, R157-R172.

[18] Toson, P.; Asali, A.; Wallisch, W.; Zickler, G.; Fidler, J. Nanostructured Hard Magnets: A Micromagnetic Study. *IEEE Trans. Magn.* **2015**, *51*, 7400104.

[19] Panagiotopoulos, I.; Fang, W.; Ott, F.; Boué, F.; Aït-Atmane, K.; Piquemal, J.-Y.; Viau, G. Packing fraction dependence of the coercivity and the energy product in nanowire based permanent magnets. *J. Appl. Phys.* **2013**, *114*, 143902.

[20] Pousthomis, M. ; Anagnostopoulou, E. ; Panagiotopoulos, I., Boubekri, R. ; Fang, W.; Ott, F ; Aït Atmane, K. ; Piquemal, J.-Y.; Lacroix, L.-M.; Viau, G. Localized Magnetization Reversal Processes in Cobalt Nanorods with Different Aspect Ratios. *Nano Res.,* **2015**, *8*, 2231-2241.

[21] Bran, C.; Ivanov, Y. P.; Garcia, J.; del Real, R. P.; Prida, V. M.; Chubykalo-Fesenko, O.; Vazquez, M. Tuning the magnetization reversal process of FeCoCu nanowire arrays by thermal annealing. *J. Appl. Phys.* **2013**, *114*, 043908.

[22] Ait Atmane, K. ; Zighem, F. ; Soumare, Y. ; Ibrahim, M. ; Boubekri, R. ; Maurer, T. ; Margueritat, J. ; Piquemal, J. –Y. ; Ott, F. ; Chaboussant, G. ; Schoenstein, F. ; Jouini, N. ; Viau, G. High temperature structural and magnetic properties of cobalt nanorods. *J. Solid State Chem.* **2013**, *197,* 297-303.

[23] Ibrahim, M.; Garcia, C.; Ait Atmane, K.; Berrichi, E.; Lacroix, L.–M.; Zwick, A.; Warot-Fonrose, B.; Lachaize, S.; Decorse, P.; Piquemal, J.-Y.; Viau, G. Carbon Coating, Carburization and High Temperature Stability Improvement of Cobalt Nanorods. *J. Phys. Chem. C* **2013**, *117*, 15808-158016.

[24] Liakakos, N.; Gatel, C.; Blon, T.; Altantzis, T.; Lentijo-Mozo, S.; Garcia-Mareclot C.; Lacroix, L.-M.; Respaud, M.; Bals, S. ; Van Tendeloo, G. and Soulantica, K. Co-Fe Nano-dumbbells : Synthesis, Structure and Magnetic Properties. *Nano Lett.* **2014**, *14*, 2747-2754.

[25] Wetz, F.; Soulantica, K.; Falqui, A.; Respaud, M.; Snoeck, E. and Chaudret, B. Hybrid Co-Au nanorods : Controlling Au nucleation and location. *Angew. Chem. Int. Ed.* **2007**, *46*, 7079-7081.

[26] Lentijo-Mozo, S.; Tan, R. P.; Garcia-Marcelot, C.; Altantzis, T. ; Fazzini, P.-F. ; Hungria, T. ; Cormary, B. ; Gallagher, J. R.; Miller, J. T.; Martinez, H.; Schrittwieser, S.; Schotter, J.; Respaud, M.; Bals, S.; Tendeloo, G. V.; Gatel, C. and Soulantica, K. Air- and Water-Resistant Noble Metal Coated Ferromagnetic Cobalt Nanorods. *ACS Nano* **2015**, *9*, 2792-2804.

[27] McGuire, M. A.; Reynolds, T. K.; DiSalvo, F. J. Crystal structure, electronic structure, and thermoelectric properties of AuTlSb: A new pyrite superstructure. *J. Alloys Compound.* **2006**, *425*, 81–87.

[28] Meng, J. F.; Polvani, D. A.; Jones, C. D.; DiSalvo, F. J.; Fei, Y.; Badding, J. V. Pressure Tuning in the Chemical Search for Improved Thermoelectric Materials: $Nd_xCe_{3-x}Pt_3Sb_4$. *Chem. Mater.* **2000**, *12*, 197–201

[29] Brown, S. R.; Kauzlarich, S. M.; Gascoin, F.; Snyder, G. J. $Yb_{14}MnSb_{11}$: New High Efficiency Thermoelectric Material for Power Generation. *Chem. Mater.* **2006**, *18*, 1873–1877.

[30] Xie, J.; Zhao, X. B.; Yu, H. M.; Qi, H.; Cao, G. S.; Tu, J. P. Low temperature solvothermal synthesis of nanosized NiSb as a Li-ion battery anode material. *J. Alloys Compd.* **2007**, *441*, 231–235.

[31] Wang, M.; Zhao, H.; He, J.; Wang, R.; Chen, J.; Chen, N. Preparation and electrochemical performance of CoSb alloy anode material for Li-ion batteries. *J. Alloys Compd.* **2009**, *484*, 864–869.

[32] Yang, Y-W.; Liu, F.; Li, T.-Y.; Chen, Y.-B.; Wu, Y.-C.,and Kong, M.-G. Electrochemical performance of template-synthesized CoSb nanowires array as an anode material for lithium ion batteries. *Scr. Mater.* **2012**, 66, 495–498.

[33] Kieslich, G.; Birkel, C. S.; Stewart, A.; Kolb, U.; Tremel, W. Solution Synthesis of Nanoparticular Binary Transition Metal Antimonides. *Inorg. Chem.* **2011**, *50*, 6938-6943.

[34] Birkel, C. S.; Kieslich, G.; Bessas, D.; Claudio, T.; Branscheid, R.; Kolb, U.; Panthöfer, M.; Raphaël, P. H.; Tremel, W. Wet Chemical synthesis and a combined X-ray and Mössbauer study of the formation of $FeSb_2$ nanoparticles. *Inorg. Chem.* **2011**, *50*, 11807-11812.

[35] Leonard, B. M.; Bhuvanesh N. S. P.; Schaak R. E. Low-Temperature Polyol Synthesis of $AuCuSn_2$ and $AuNiSn_2$: Using Solution Chemistry to Access Ternary Intermetallic Compounds as Nanocrystals. *J. Am. Chem. Soc.* **2005**, *127*, 7326-7327.

[36] Cable, R. E.; Schaak, R. E. Low-Temperature Solution Synthesis of Nanocrystalline Binary Intermetallic Compounds Using the Polyol Process. *Chem. Mater.* **2005**, *17*, 6835-6841.

[37] Soumare, Y.; Garcia, C.; Maurer, T.; Chaboussant, G.; Ott, F.; Fiévet, F.; Piquemal, J.-Y.; Viau, G. Kinetically controlled synthesis of cobalt nanorods with high magnetic coercivity. *Adv. Funct. Mater.* **2009**, *19*, 1971-1977.

[38] Ishida, K.; Nishizawa, T. The Co-Sb (Cobalt-Antimony System). *Bull. Alloy Phase Diagrams*. **1990**, *11*, 243-248.

[39] Dugay, J.; Tan, R.P. ; Ibrahim, M. ; Garcia, C.; Carrey, J. ; Lacroix, L.-M. ; Fazzini, P.-F. ; Viau, G. ; Respaud. M. Charge transport and interdot coupling tuned by the tunnel barrier length in assemblies of nanoparticles surrounded by organic ligands. *Phys. Rev. B rapid commun.* **2014**, *89*, 041406(R).

[40] Viau, G. ; Garcia, C. ; Maurer, T. ; Chaboussant, G. ; Ott, F. ; Soumare, Y. ; Piquemal, J.-Y. Highly crystalline cobalt nanowires with high coercivity prepared by soft chemistry. *Phys. Status Solidi* A **2009**, *206*, 663-666.

[41] Amornpitoksuk, P.; Ravot, D.; Mauger, A.; Tedenac, J. C. Structural and magnetic properties of the ternary solid solution between CoSb and $Fe_{1+\delta}Sb$. *Phys. Rev. B* **2008**, *77*, 144405.

Supplementary Information

Co@CoSb core-shell nanorods: from chemical coating at the nanoscale to macroscopic consolidation

Udishnu Sanyal [a] *Semih Ener,*[b] *Evangelia Anagnostopoulou* [a] *Marc Pousthomis,*[a] *Pier-Francesco Fazzini,*[a] *Lise-Marie Lacroix,*[a] *Konstantin P. Skokov,*[b] *Oliver Gutfleisch,*[b] *and Guillaume Viau* [a,*]

[a] Université de Toulouse, Laboratoire de Physique et Chimie des Nano-Objets, UMR 5215 INSA, CNRS, UPS, 135 avenue de Rangueil, F-31077 Toulouse cedex 4, France

[b] Funktionale Materialien, Institut für Materialwissenschaft, TU Darmstadt, 64287 Darmstadt, Germany

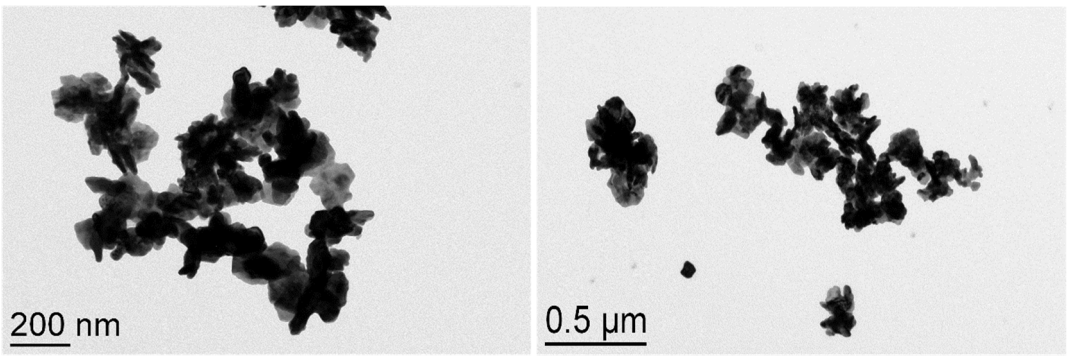

Figure S1. TEM images of CoSb NPs prepared by the reduction of a mixture of antimony acetate and cobalt acetylacetonate in a solution of oleylamine containg tetradecanediol.

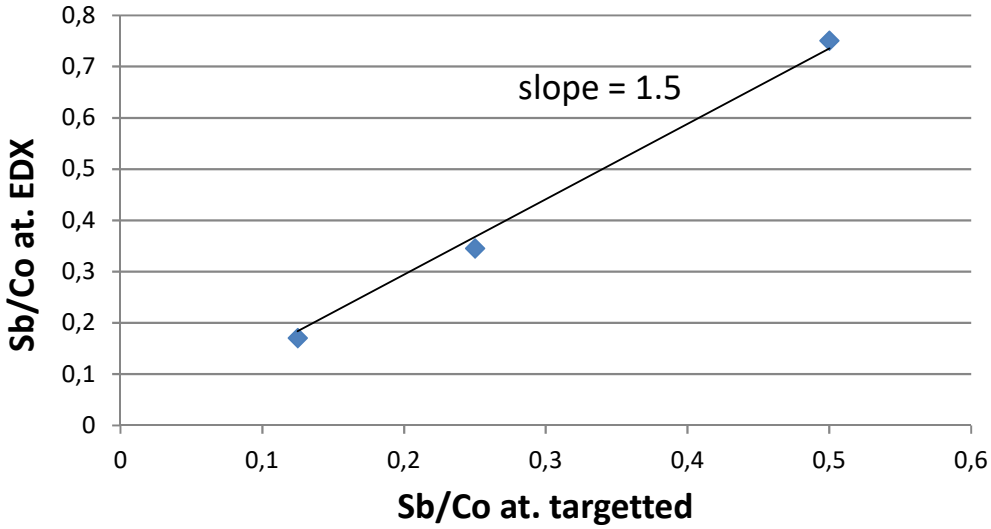

Figure S2. Sb/Co atomic ratio measured in the powders prepared by reaction of antimony(III) acetate with Co nanorods vs the Sb/Co ratio in the starting mixtures.

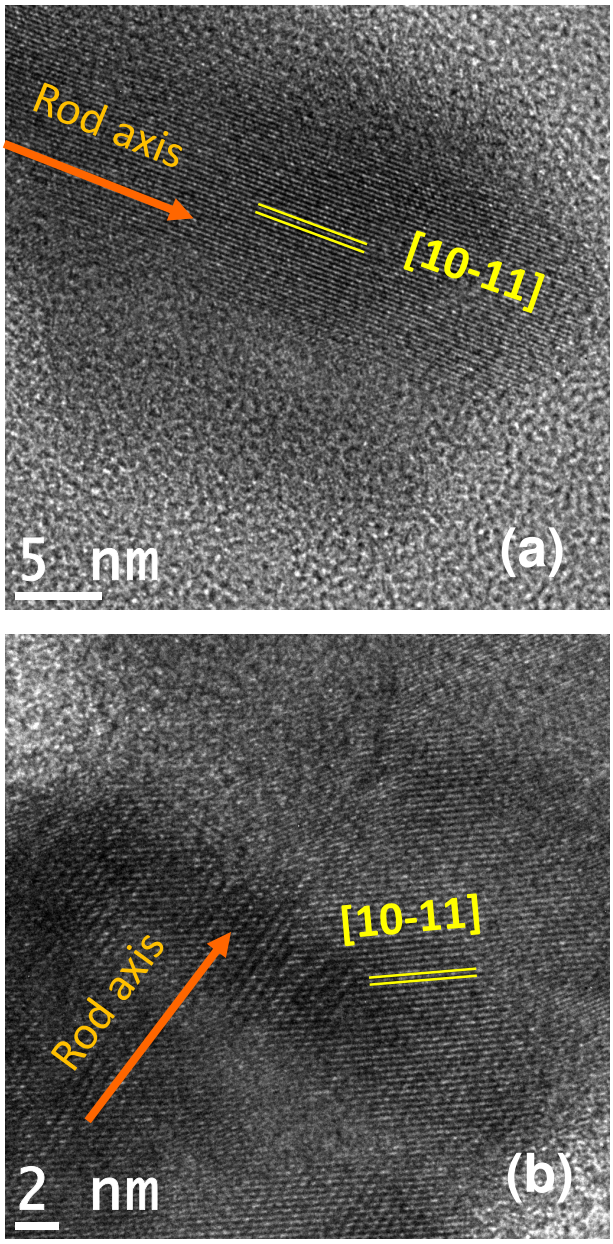

Figure S3. HRTEM images of Co@CoSb nanorods prepared with a Sb/Co ratio of 1/4. The lattice fringes corresponding to the {10-11} planes spread across the entire images but their orientations with respect to the rod axis are different.

Annealing experiments

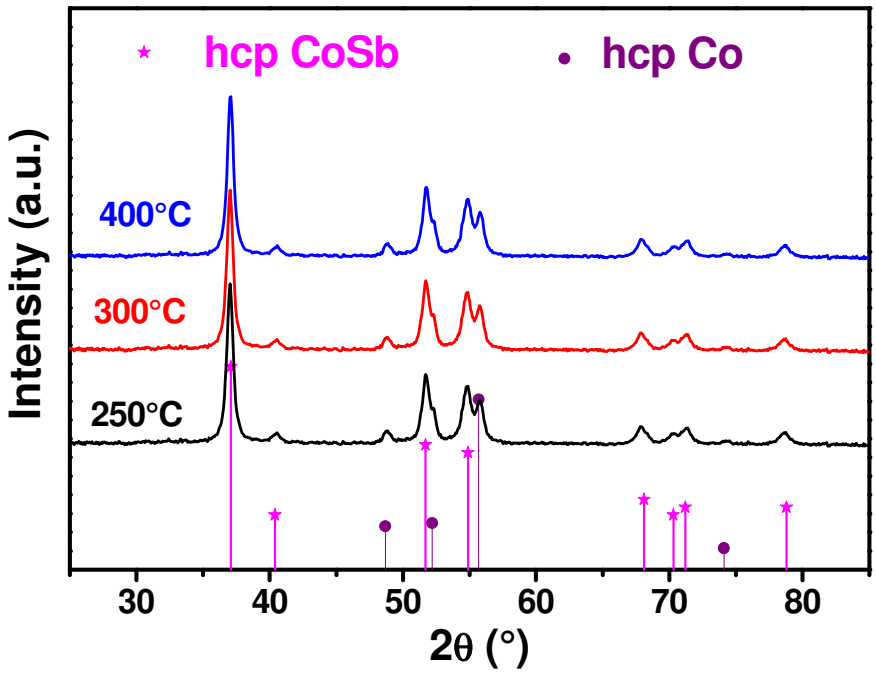

Figure S4. Room temperature XRD pattern of the $Co_{50}@(Co_{0.5}Sb_{0.5})_{50}$ nanorods annealed in H_2/N_2 atmosphere (H_2 content = 7%) at different temperatures.

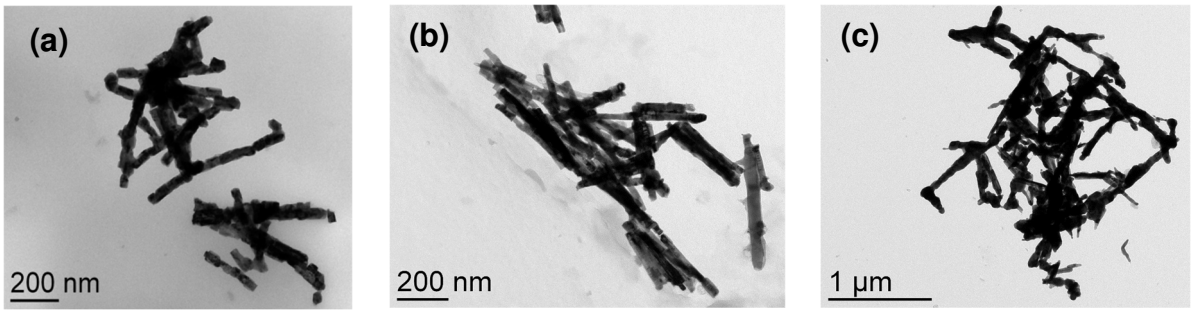

Figure S5. TEM image of the $Co_{50}@(Co_{0.5}Sb_{0.5})_{50}$ particles annealed at different temperatures: (a) 250°C; (b) 300°C; (c) 400°C.

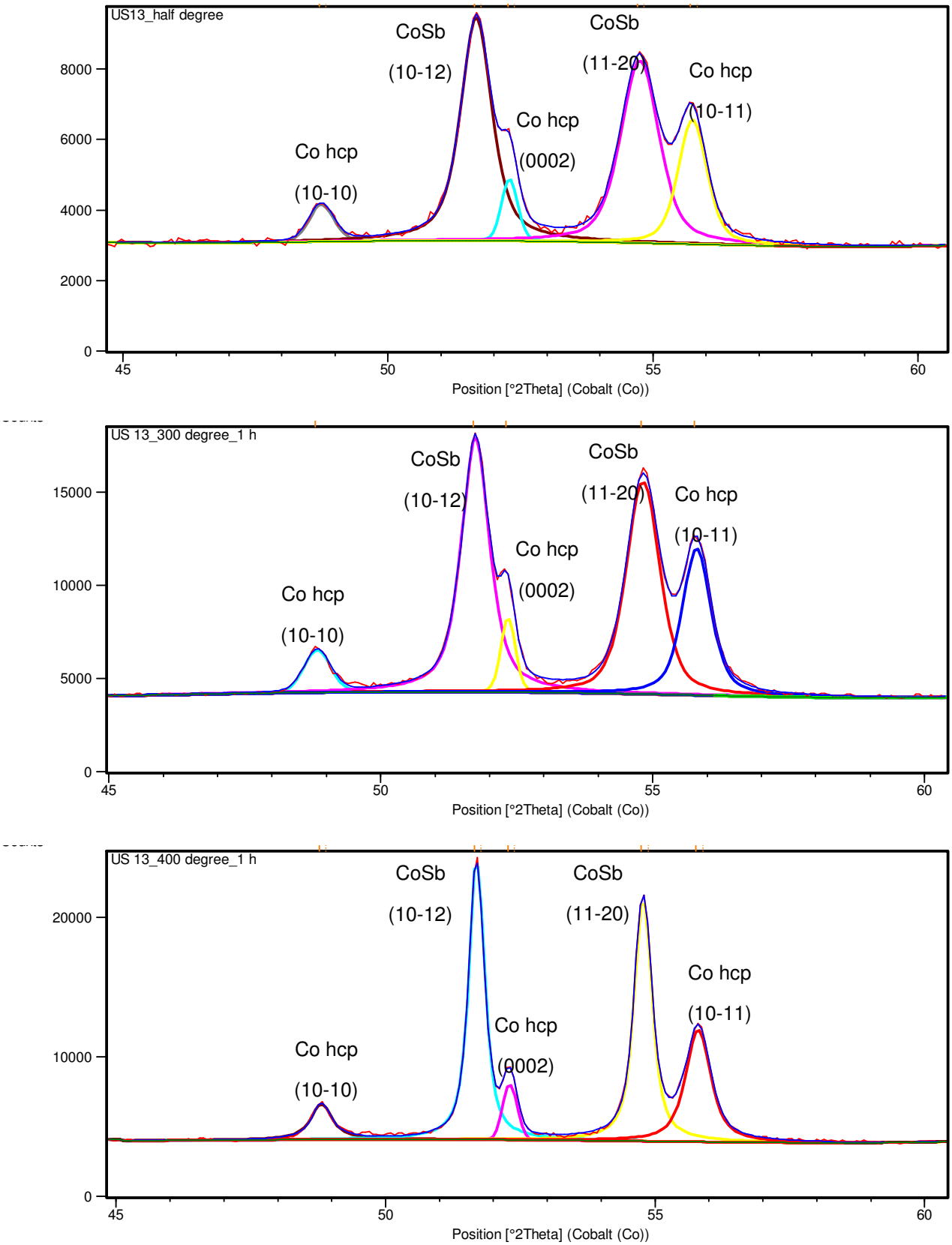

Figure S6. Room temperature XRD patterns of the $Co_{50}@(Co_{0.5}Sb_{0.5})_{50}$ powder: raw particles and particles annealed at 300°C and 400°C for 1h under forming gas.

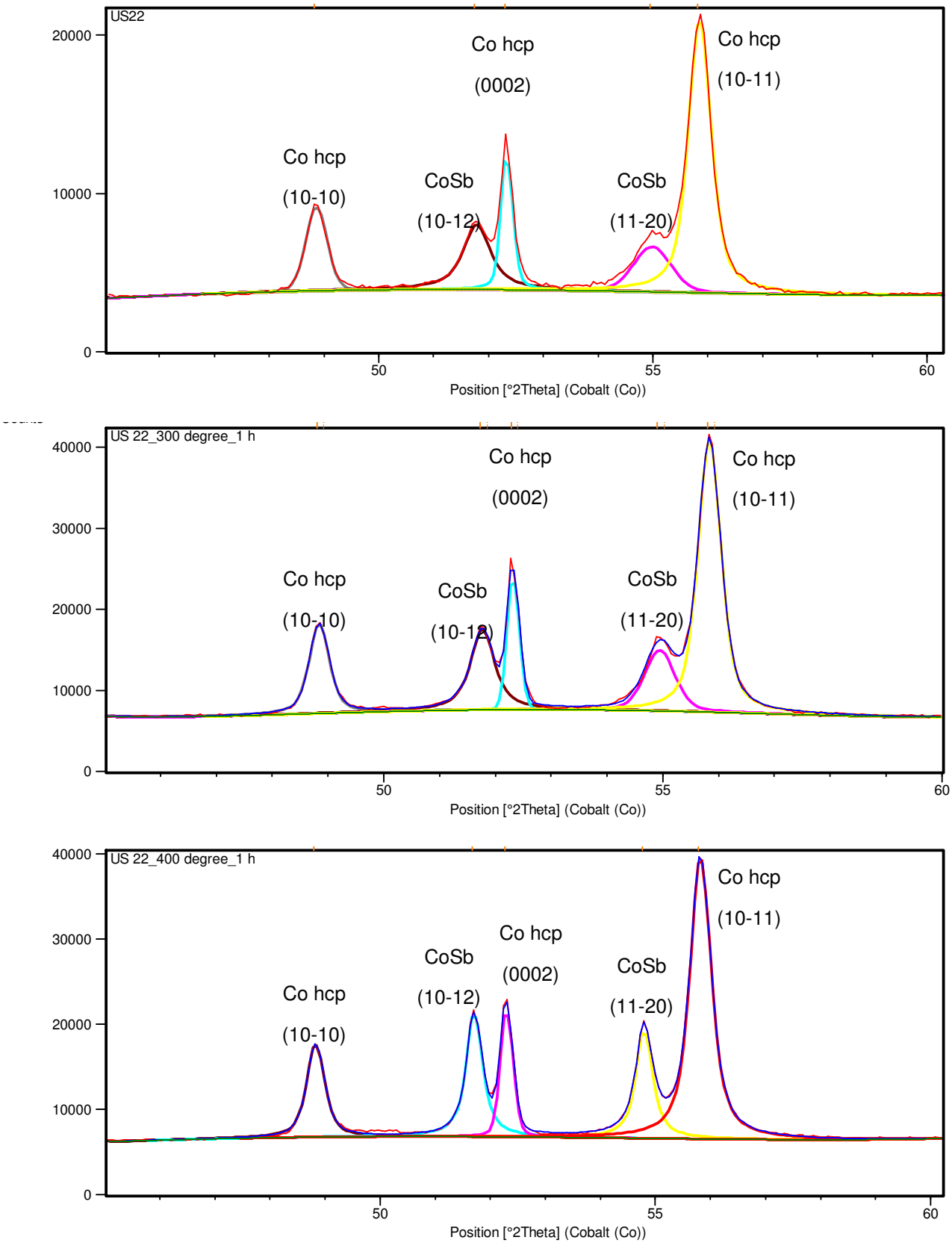

Figure S7. Room temperature XRD pattern of the $Co_{70}@(Co_{0.5}Sb_{0.5})_{30}$ powder, raw particles and particles annealed at 300°C and 400°C for 1h under forming gas.

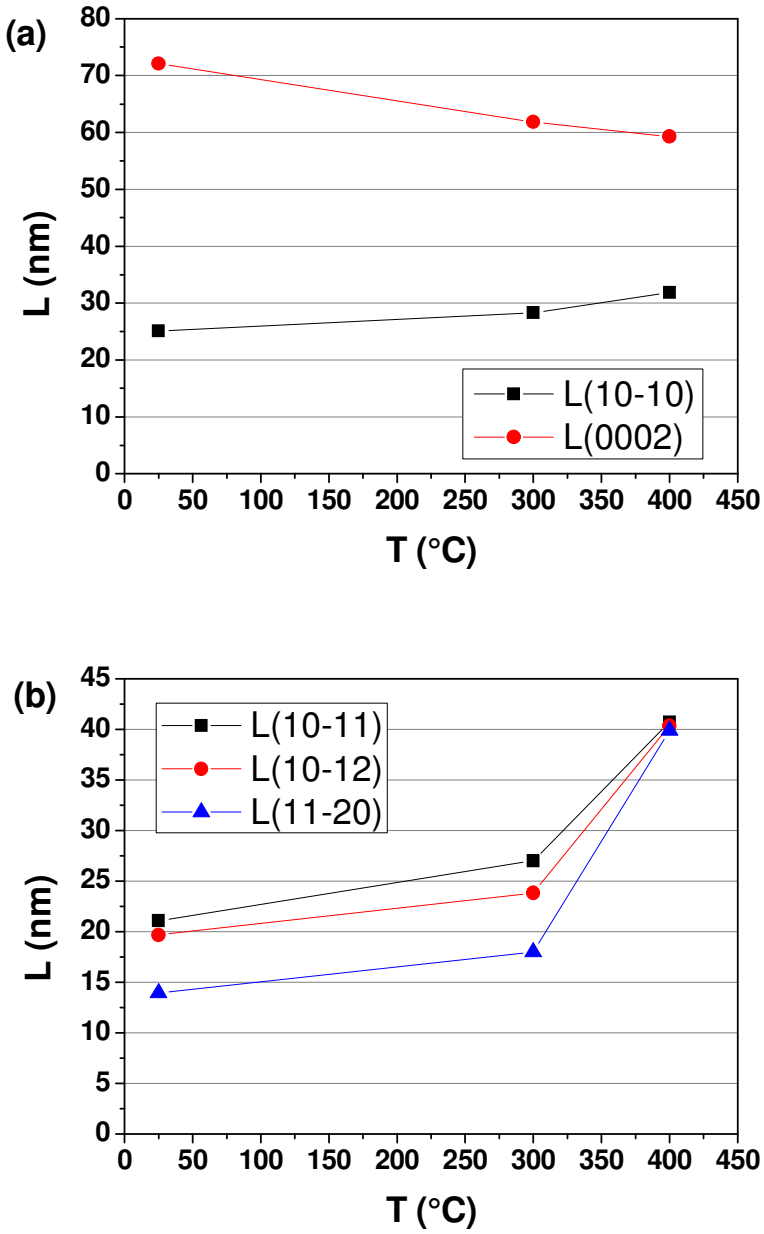

Figure S8. Crystallite size measured on the XRD pattern of $Co_{70}@(Co_{0.5}Sb_{0.5})_{30}$ particles after annealing under forming gas at different temperatures : (a) for the hcp Co phase, perpendicular and parallel to the *c* axis calculated from the (10-10) and (0002) line broadening, respectively ; (b) for the reflections (10-11), (10-12) and (11-20) of the β-CoSb phase.

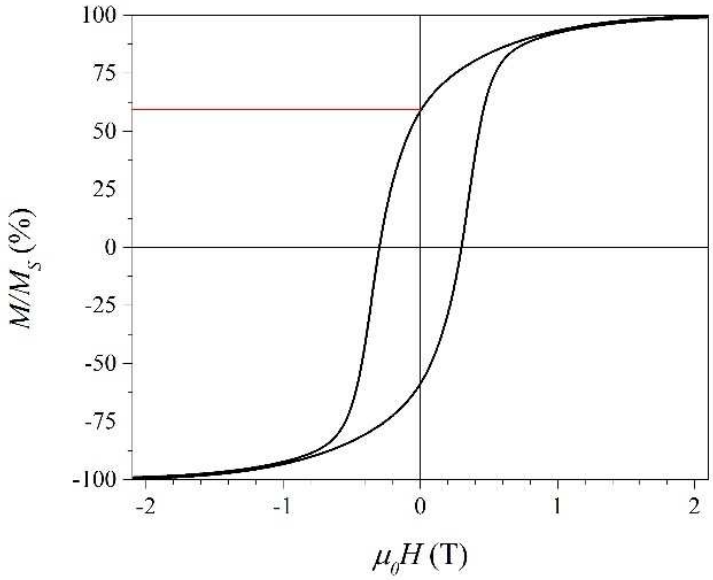

Figure S9. Room temperature magnetization loop of a magnet made by the hot compaction of $Co_{70}@(Co_{0.5}Sb_{0.5})_{30}$ nanorods (measurement with a pulse magnetometer). The magnetization curve was measured with the applied magnetic field parallel to the field direction that was applied to pre-align the rod before compaction.